Optical Performance Prediction of the Thirty Meter Telescope after Initial Alignment Using Optical Modeling

Byoung-Joon Seo[a], Carl Nissly[a], Mark Colavita[a], Mitchell Troy[a],
Scott Roberts[b], and John Rogers[b]

[a] Jet Propulsion Laboratory, California Institute of Technology, Pasadena, CA. 91109
[b] Thirty Meter Telescope Observatory, Pasadena, CA. 91107

ABSTRACT

We present an estimate of the optical performance of the Thirty Meter Telescope (TMT) after execution of the full telescope alignment plan. The TMT alignment is performed by the Global Metrology System (GMS) and the Alignment and Phasing System (APS). The GMS first measures the locations of the telescope optics and instruments as a function of elevation angle. These initial measurements will be used to adjust the optics positions and build initial elevation look-up tables. Then the telescope is aligned using starlight as the input for the APS at multiple elevation angles. APS measurements are used to refine the telescope alignment to build elevation and temperature dependent look-up tables. Due to the number of degrees of freedom in the telescope (over 10,000), the ability of the primary mirror to correct aberrations on other optics, the tight optical performance requirements and the multiple instrument locations, it is challenging to develop, test and validate these alignment procedures. In this paper, we consider several GMS and APS operational scenarios. We apply the alignment procedures to the model-generated TMT, which consists of various quasi-static errors such as polishing errors, passive supports errors, thermal and gravity deformations and installation position errors. Using an integrated optical model and Monte-Carlo framework, we evaluate the TMT's aligned states using optical performance metrics at multiple instrument and field of view locations. The optical performance metrics include the Normalized Point Source Sensitivity (PSSN), RMS wavefront error before and after Adaptive Optics (AO) correction, pupil position change, and plate scale distortion.

Keywords: Thirty Meter Telescope, Optical Modeling, Alignment and Phasing System, Optical Performance

1. INTRODUCTION

The use of segmented mirrors is a key innovation of many modern large-aperture telescopes such as Thirty Meter Telescope (TMT). Although this segmented approach surely avoids the difficulty of fabricating one large monolithic mirror, the complexity added by multiple segments needs to be overcome by precise alignment and control. We estimate the optical performance of the TMT after execution of the initial telescope alignment plan.

We have developed and updated an integrated optical model of the TMT for system engineering performance and sensitivity analyses.[1–3] The model includes static optical surface errors and rigid body (RB) errors of the primary mirror segments, the secondary, and tertiary mirrors. It also has a model of initial telescope alignment subsystems such as the Global Metrology System (GMS) and the Alignment and Phasing System (APS). The integrated model allows for simulation of the TMT before and after correction of the telescope wavefront. Using this model, we have reported the optical performance impact of individual errors previously.[2,3] The modeling results have been updated as the modeling becomes mature for the error budgeting purpose managed by the TMT system engineering group.[4] In this paper we evaluate the final optical performance metrics after execution of the proposed TMT initial alignment plan on multiple realizations of initial TMT telescopes.

As described in Sec. 4, the TMT initial alignment is performed by GMS, M1 Control System (M1CS), and APS. The GMS first measures the RB locations of the telescope optics (M1, M2, and M3), and instruments as a function of elevation angle. These initial measurements will be used to adjust the optics' positions and build initial elevation look-up tables. Then the telescope is aligned using starlight as the input for the APS at multiple

elevation angles. The APS measurements are used to refine the telescope alignment and build elevation (and potentially temperature) dependent look-up tables. During all these processes, all segments need to be aligned, which is done by the M1CS. Due to the number of degrees of freedom in the telescope (over 10,000), the ability of the primary mirror to correct aberrations on other optics, the tight optical performance requirements and the multiple instrument locations, it is challenging to develop, test and validate these alignment procedures.

We apply the alignment procedure to the model-generated TMTs. Using an integrated optical model and Monte-Carlo framework, we evaluate TMT aligned states using optical performance metrics at multiple instruments, zenith angles, and field of view locations. The optical performance metrics include the Normalized Point Source Sensitivity (PSSN), the RMS wavefront error (rmsWFE) before and after alignment, the pupil position, the image motion, and the plate scale distortion. We explicitly define these metrics in Appendix A.

This paper is organized as follows. In Sec. 2, we provide an overview of the TMT instrument or subsystems, which participate the TMT alignment. In Sec. 3, we describe our modeling of the TMT before the alignment plan is executed. We present the current TMT alignment procedure in Sec. 4 with assumptions we have made for the modeling purpose. In Sec. 5, we present optical performance results after the baseline scenario as well as some useful scenarios are executed. Lastly in Sec. 6, we conclude by discussing our future works.

2. OVERVIEW OF ALIGNMENT INSTRUMENTS

2.1 GMS

The GMS is a TMT subsystem, which is responsible for initial coarse alignment of the TMT. The GMS consists of three (To Be Determined (TBD)) laser trackers and 6 targets located around the perimeter of M1, 6 targets around the central hole in M1, 4 targets on the M2 support, 4 targets on the M3 baffle, and 3 targets on each instrument. The GMS performs metrological survey of the telescope structure both before and after installing optics by varying the observatory azimuthal and elevation axes.

The GMS will generate initial Look-Up-Table (LUT) for M2, M3 and instruments' 6 Degree of Freedom (DoF) locations. We call this the "GMS LUT" throughout this paper. Due to the lack of fiducials on M1 segments, the GMS can not measure the individual M1 segment positions. However, with fiducials around the outer and inner segments edges, a relation is established between the telescope global coordinate systems and the global M1 coordinate system such as M1 Reference Coordinate System (M1RCS).

The GMS will use a laser tracker system such as the API radian laser Tracker*. The quoted accuracy of a single laser tracker is the greater of $\pm$ 10 µm or 5 ppm (2 sigma). The angular accuracy is quoted as 3.5 µm/m (assumed also 2 sigma). Using these values together with the currently planned laser tracker location, number of targets and their locations, Rogers estimated the accuracy of each TMT optics RB location.[5] The GMS accuracy we consider in this study is based on ideal assumptions such as all GMS targets are visible and ideally installed with no errors with respect to optics surfaces, excluding any locational errors of the GMS laser tracker, targets and the optical surfaces or instrument focal surfaces. The study can be repeated using spatial analyzer software to confirm that these estimates are achievable in practice.

We use the result from [5] for our assumption for the M2 and M3 status after the GMS alignment, which is summarized later in Table 2.

2.2 APS

The APS is a TMT instrument mounted on the nasmyth platform. The APS is responsible for the precision optical alignment of the TMT. The APS consists of various Shack Hartmann (SH) Wavefront Sensors (WFSs) to measure the telescope wavefront to estimate the shape and the position of the optical surfaces. Based on these APS measurements at various different zenith telescope pointing angles, the Telescope Control System (TCS) generates a LUT for segment Warping Harness (WH) commands, segment Piston, Tip, and Tilt (PTT) positions, M2 PTT positions and M3 Tip and Tilt (TT) positions. We call this LUT "APS LUT" throughout this paper. The APS LUT is generated when the telescope is initially aligned and updated as needed typically every few

*http://www.apisensor.com/products/radian/

weeksTo Be Reviewed (TBR). The APS is designed after the Phasing Camera System (PCS), which performed most of these tasks for the Keck Telescopes.

The APS has several operating modes for different optical calibrations such as segment phasing, segment TT, segment WH calibration. Chanan, et. al., have predicted the measurement uncertainties of the APS based upon empirical data from the PCS of the Keck Telescopes, scaling them as appropriate to the TMT.[6] Chanan, et. al., found that the residual segment alignment uncertainty is dominated by the atmospheric residual, which is proportional to the diameter of the telescope Entrance Pupil (EnP) aperture diameter and the exposure time.

In this study, we add these measurement uncertainties in the form of an atmospheric phase screen, scaled by the integration time in each exposure of the APS measurement. We refer to this noise as "Atmospheric Phase Residual Noise" or simply "atmospheric noise" or "APS noise". In addition to this atmospheric noise, we include the APS segment phasing error of 6.8 nmRMS surface, which is the current APS phasing requirement after the fine phasing. The APS will employ "broadband and narrowband phasing algorithms" for coarse and fine phasing of the segments.[6,7]

2.3 M1CS

The TMT primary mirror is comprised of 492 hexagonal mirror segments. The relative segment positions are measured using capacitance edges sensors, two per edge, from which the mirror shape is reconstructed. Deviations from the desired shape are controlled using 3 actuators per segment. This maintenance task is the responsibility of M1CS;[8] establishing the desired shape is the responsibility of APS.

Because of in-plane motion of the segments with gravity and temperature, finite sensor installation errors result in cross terms from in-plane motion to measured height, in addition to ordinary zero-point errors. To accommodate these errors, the edge sensors measure the relative height (combined with dihedral angle) as well as the gap between sensors. From the ensemble of gap data, the actual in-plane motion can be determined. These in-plane measurements along with the measured heights are then used as inputs to a sensor calibration model to correct for the zero point and the cross terms.[9] To solve for the coefficients of the model, APS measurements are performed at several elevation angles following each segment exchange.

Errors in the achieved M1CS performance are attributable to calibration residuals, sensor random noise, sensor drift between APS runs, actuator random noise, and disturbances from wind and vibration. Neglecting the random noise and disturbance terms, the quasistatic contribution of M1CS to the overall PSSN budget is better than 0.99. Throughout this paper and discussed again in ***A1*** in Sec. 4.1, we exclude any performance impact associated with M1CS. Since its effects should be statistically uncorrelated with those described below, the M1CS impact can be treated as an independent contributor to the total image quality metrics.

3. TMT MODEL BEFORE ALIGNMENT

Table 1 lists the initial static error terms included before we apply the alignment plan. They are optical surface errors and rigid body errors of the primary mirror segments, the secondary and tertiary mirrors. They also include the rigid body misalignment of instrument. These errors are the subset of TMT error budget[10] excluding time-dependent dynamic error terms such as thermal and dome seeing, vibration, wind residual and etc. We have evaluated the optical impacts of these errors for the TMT system engineering performance and sensitivity analyses using our integration optical model.[2,3] Fig. 1 show example Optical Path Differences (OPDs) of several error terms before they are aligned when the telescope is pointing at 45 degree. Fig. 1(a) and Fig. 1(b) are for the "M1 Passive Support error" for axial and later components, respectively, and Fig. 1(c) is for the "M1 Figuring error" after final polishing. Fig. 1(d) and Fig. 1(e) are the OPDs for M1 combined and M2 combined cases when all the checked errors under M1 or M2 surface errors and RB motions are combined as indicated in Table 1. Note that the GMS errors are excluded in M1 and M2 combined cases, which are separately included under the LUT error. Fig. 1(f) is the OPD for "all combined errors" when all of the checked errors are combined in Table 1. We assume that the telescope states of all combined errors are the initial telescope states before the TMT alignment plan is executed.

Description of these individual error terms is not the scope of this paper. Our previous report described most, but not all, error terms.[2,3] For complete description, we refer our optical error manual in our controlled document database at the TMT project office.[4]

Table 1: Initial static error terms included before we apply the alignment plan. They are optical surface errors and rigid body errors of the primary mirror segments, the secondary and tertiary mirrors. They also include the rigid body misalignment of instrument under the LUT error.

M1	Segment Support Print Through (SSPT)	Axial Gravity
		Lateral Gravity
	Segment In-Plane Displacement (SIPD)	Gravity STR Mirror cell
	Segment Thermal Distortion (STD)	Segment Thermal Distortion
		Segment Thermal Clocking
	Segment Residual Figure Error (SRFE)	Segment Vendor
		Ambient Testing
M2	M2 Support Print Through (M2SPT)	Axial Gravity
		Lateral Gravity
	M2 Residual Figuring Error (M2RFE)	High Order Residual (HOR)
M3	M3 Support Print Through (M3SPT)	Axial Gravity
	M3 Residual Figuring Error (M3RFE)	HOR
LUTE	Look-Up-Table Error	GMS LUT Error
		APS LUT Error
WFS	M1 Segment Phasing Wavefront Measurement Error (WFSSP)	
	M1 Segment Tip/Tilt Measurement Error (WFSTT)	
	Low Order Wavefront Measurement Error (WFSLO)	
	M1 Warping Harness Wavefront Measurement Error (WFSWH)	

4. TMT ALIGNMENT PROCEDURE

We describe the TMT alignment procedure and assumptions in this section. The complete alignment procedure for the TMT is under development. A potential alignment procedure and assumptions are described in this paper only for modeling purpose.

The TMT alignment is performed by the GMS, the M1CS and the APS. As discussed in Sec. 2, GMS initiates the coarse alignment followed by fine alignment by the APS. At each APS calibration, the M1CS records the segments edge sensor offset positions and maintains the relative segment positions. The GMS and the APS will have their LUTs while the M1CS will use a mathematical fit rather than a LUT.

Sec. 4.1 first highlights our key assumptions in the considered TMT alignment procedure. Then, Sec. 4.2 describes each step in more detail.

4.1 Key assumptions

Below lists our key assumptions regarding the considered TMT alignment process.

A1 **Perfect M1CS**:

We assume that the M1CS is working perfectly. It is analogous that the M1CS is working with an infinite number of edge sensors (no degeneracy) and with no measurement error. This is assumed throughout this report. The M1CS maintains the segment out-of-plane motions according to its initial "as-is" edge sensor readings and monitors the segment in-plane motions. (There are no in-plane motion actuators.) Then, segments are aligned relative to each other within only edge sensor alignment error. We implement this edge sensor alignment error as M1 segment out-of-plane, PTT, errors as described in Step (3) below.

A2 **Discrete zenith angle LUT**:

The GMS and the APS are calibrated at discrete zenith angle locations. The zenith angles used for LUTs are [5, 15, 30, 45, 60] degrees. This is somewhat arbitary choice at this moment considering normal telescope operation range from 5 degree to 65 degree.

A3 **APS LUT**:

The APS LUT includes the segment WH actuator positions which are computed when the TMT is configured at the APS instrument position, On-Axis, and at a zenith angle of 30 degrees. This simulates the act of setting the WH at a single telescope zenith angle, which is the TMT baseline procedure. These WH commands are stored at the time of calibration and applied to the telescope until the next calibration. These WH commands are independent of zenith angle, instrument position and delta temperature.

The APS LUT also includes the segment PTT positions, the M2 PTT positions and, the M3 TT positions, which are computed at the APS instrument position for the zenith angles specified by ***A2***. These rigid-body commands are stored at the time of calibration and applied to the telescope until next calibration. These rigid-body commands are independent of instrument position and delta temperature. When the telescope is pointing the zenith angle other than ***A2***, we use the actuator positions interpolated from the LUT. We

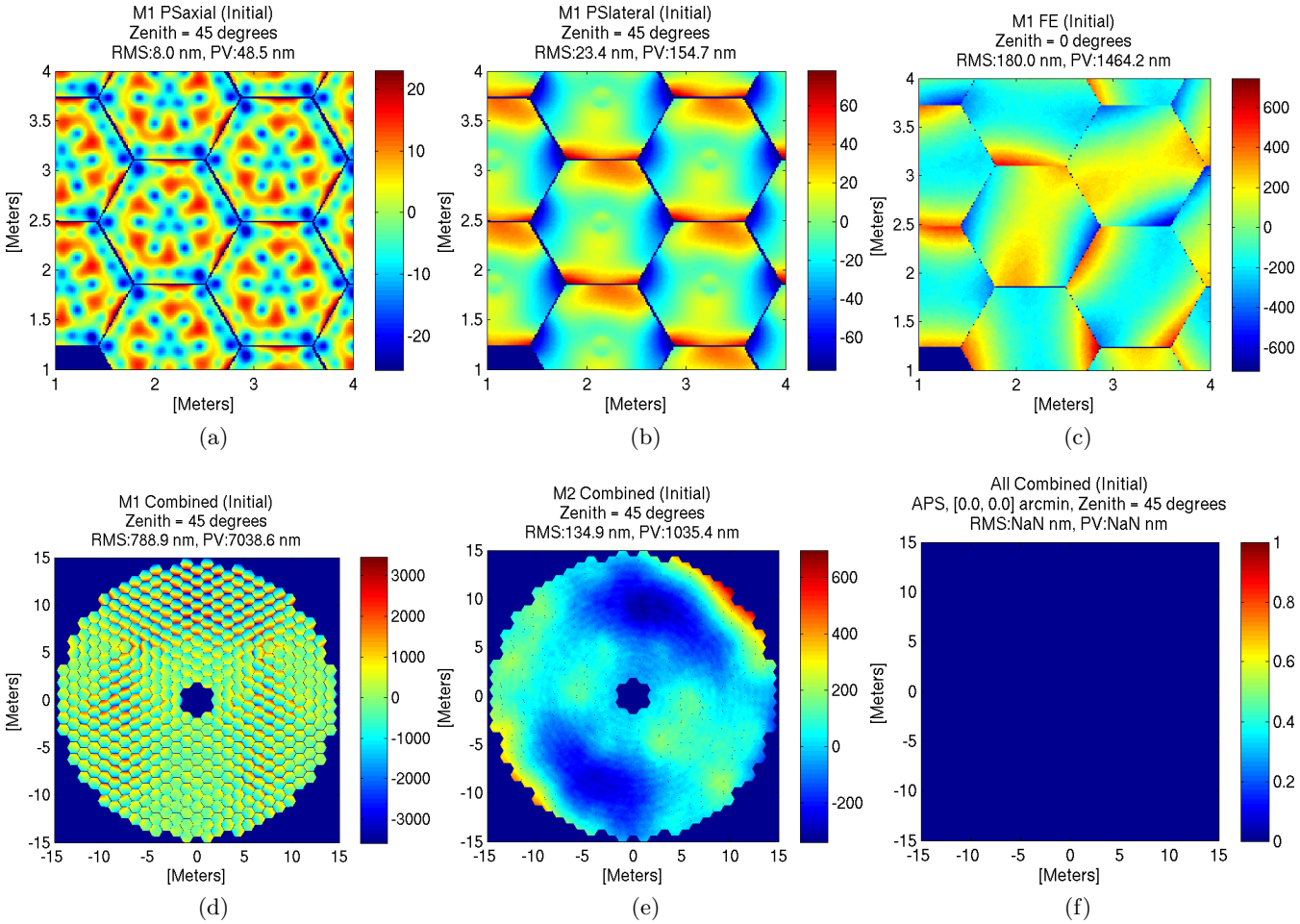

Figure 1: Example OPDs of several error terms before they are aligned. Telescope is assumed pointing at zenith angle of 45 degree. (a) and (b) are for the "M1 Passive Support error" for axial and later components, respectively, and (c) is for the "M1 Figuring error" after final polishing. (d) and (e) are the OPDs for M1 combined and M2 combined cases when all the checked errors under M1 or M2 surface errors and RB motions are combined as indicated in Table 1. (f) is the OPD for "all combined errors" when all of the checked errors are combined in Table 1.

use "3rd order polynomial interpolation" based on our separate case study. (Detail is not included in this paper.)

We also assume that the 5-rings per segment Shack Hartmann Wavefront Sensor (SH-WFS) is used for the APS wavefront sensing. This 5-ring SH-WFS has 91 hexagonal sub-apertures per segment, with 28 cm subapertures from corner-to-corner in entrance pupil space. Over the 492 M1 segments, this works out to be 44,772 SH subimages across the pupil. Our model samples the wavefront as seen by each sub-aperture, fitting tip and tilt to each sample to measure slope. The dominant noise source from the SH-WFS measurement is residual atmospheric error. To simulate this effect, a long exposure phase screen[6,11] is added to the calculated telescope wavefront prior to the SH-WFS slope measurement. An effective integration time of 240 second is assumed for the measurement error. This model includes the effects of atmospheric noise, spatial sampling and aliasing of the SH-WFS. The model does not include relatively minor effects such as centroiding errors or CCD sampling.

A4 **On-Instrument Wavefront Sensor (OIWFS)**:

Each instrument has its own OIWFS, which is used to adjust M2 PTT as a final alignment step. The OIWFS is assumed to sense up to the fourth order Zernikes Wavefront Error (WFE) (up to 15th Noll Zernike mode.)

We also assume that all OIWFSs are located On-Axis. Since we assume a flat detector plane at this moment, we are not capturing the relative defocus change between on and off Field of View (FoV). We plan to update this considering the curved detector surface in the future with a correct OIWFS location for each instrument.

A5 **M3 TT follows the GMS LUT**:

When M3 is pointed to an instrument other than APS, the M3 TT is adjusted based on its GMS LUT, not the APS LUT. (See our study Sec. 5.2 for this choice).

A6 **No pointing model**:

After the telescope is initially assembled and aligned, empirical star locations are collected in the acquisition camera on each instrument while the telescope is pointed to various known acquisition stars at various zenith and horizon angles in the sky. Based on this star acquisition data, an empirical model will be established to acquire a star at an any arbitrary zenith, horizontal angle and instrument. We define this model as "pointing model" for the telescope.

This pointing model is an important building block acquiring and guiding a target star in the sky . We also define "pointing error" as any discrepancy between actual star position in the sky and the conceived position of the star by this pointing model. The pointing error is the measure of quality of this pointing model, which should be budgeted and controlled.

It is beyond our study scope to simulate this pointing model and estimate the pointing error. We assume no pointing model in this study. We assume the full telescope are tilted or rotated perfectly as the zenith and horizon angles are changed and an arbitrary star is exactly located at the known position with no knowledge error. The pointing error should be distinguished from the star centroid error or image motion, which are defined in Appendix A and are used in Sec. 5.

4.2 Alignment Steps

The TMT alignment steps are summarized below.

(1) Mirror installation

- Key procedure:
  All optics (M1 segments, M2, and M3) and all instruments are assembled and installed.

- Modeling assumption:
  In practice, only a subset of M1 segments may be installed and the TMT will be operated/aligned with such a partial segment-installation state. However, we do not consider this partial segment installation state here. We assume all optics and the APS are installed with the GMS capture range. (The GMS capture range is unknown to us.) We also assume that the telescope is pointing to zenith when all optics are installed.

(2) M1CS initialized and turned on

- Key procedure:
  The initial set points for the M1CS edge sensors are their "as-is" values. M1CS feedback control loop is on.
- Modeling assumption:
  We assume M1CS is working perfectly as we described in ***A1*** in Sec. 4.1. The accuracy of the M1 segment alignment depends on the edge sensor installation error, which is discussed in Step (3) below.

(3) Initial alignment at Zenith

- Key procedure:
  All M1 segments, M2, M3 and all instruments are aligned coarsely.
- Modeling assumption:
  This initial alignment is done in with respect to the telescope global coordinate such as Elevation structure Coordinate Reference System (ECRS).[12] Thus, this step determines the relationship between the telescope global coordinate systems to each mirror's local coordinate system. Due to the lack of the fiducials on M1 segments, the GMS cannot measure the individual M1 segment positions. However,

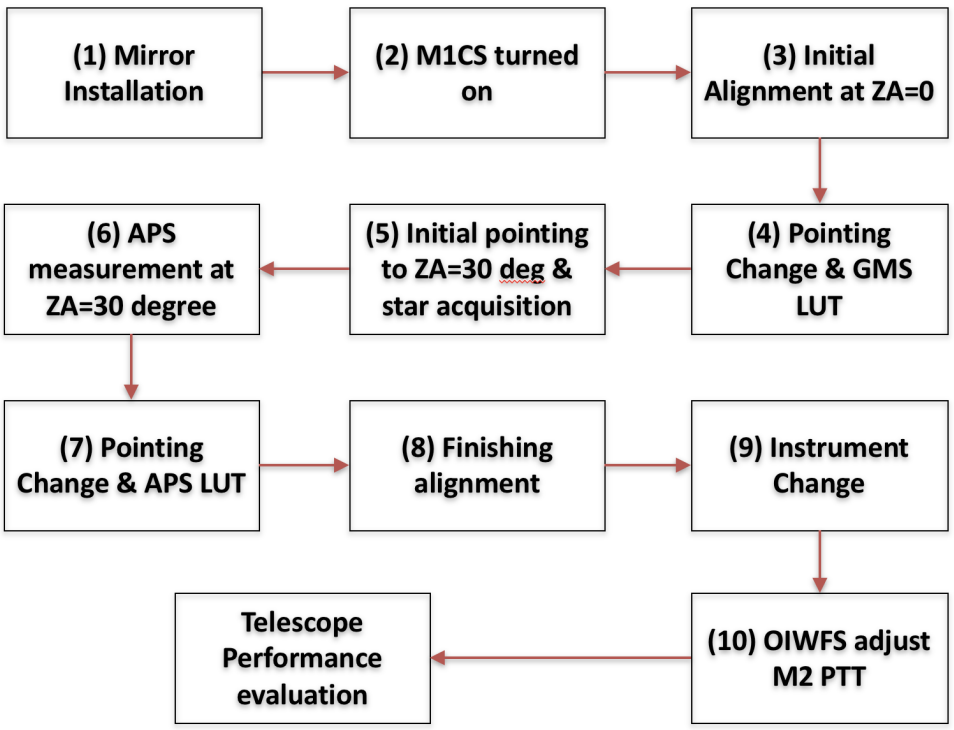

Figure 2: Telescope alignment procedure considered in this study. The complete alignment procedure for the TMT is under development. An potential alignment procedure and assumptions are described in this paper only for modeling purpose.

with fiducials around outer and inner segments edges as discussed in Sec. 2.1, the relation is established between the telescope global coordinate systems and the global M1 coordinate system such as M1RCS. Although APS has three GMS targets (Sec. 2.1), we assume we do not utilize the GMS measurement on the APS or any instrument. We assume either the detector location uncertainty with respect to the GMS targets is worse that the GMS measurement uncertainty or that the GMS measurement uncertainty is larger than the instrument installation error.

After this coarse alignment, Table 2 summarizes misalignment with respect to the global coordinate system. We assume all optics (M1 492 segments and M2, M3) and all instruments are randomly independently misaligned with Gaussian distribution with zero mean and standard deviations of values in Table 2. M2 and M3 are aligned by GMS, for which, we use the GMS estimated accuracy[5] as we discussed in Sec. 2.1. Due to the lack of the fiducials on M1 segments, M1 segment alignment is excluded. M1 segment out-of-plane positions (PTT) are determined by the M1CS edge sensor installation errors. For M1 segment TT, the Current Best Estimation (CBE) of the M1CS edge sensor installation accuracy was used. This is $\pm$ 15 arcsecon $-$ sky, which is equivalent to 50 µrad. For M1 segment z position (piston), M1CS edge sensor installation accuracy of $\pm$ 30 µm was used. For M1 segment in-plane motions (translation and clocking), we consider the CBE of the segment installation errors.[13]

For instruments, we consider the CBE of Narrow-Field Infrared Adaptive Optics System (NFIRAOS) installation errors for the coarse alignment accuracy from the Interface Controlled Document (ICD) between Telescope Structure System (STR) and NFIRAOS.[14] We have interpreted its position error as "The NFIRAOS focal plane center will be within a sphere of 10 mm radius from the nominal position." and its orientation as "NFIRAOS will point to the middle of M3 within a 10 mm radius circle. This circle is located at the M3 center surface and perpendicular to the nominal NFIRAOS optical axis." Therefore, for the instrument' translation errors, we generate a 3D random point using the spherical coordinate with radius of 10 mm as indicated in $^+$. Likewise, for the instruments' rotational errors, we use the cylindrical coordinate for the pitch/yaw errors as indicated in $^+$.

Note that, for M2 and M3, the sensing error (GMS measurement error) is assumed to be dominant over their installation/adjustment. Thus, M2 and M3 have designed positions, measured positions, and their knowledge errors in measured positions. On the other hand, we assume we do not rely on the GMS measurements in locating the M1 segments and instruments, thus, they have only the installation errors but no measured positions.

The GMS measurement and installation errors may both have deterministic bias errors (difference between ideal and measured location) and measurement errors (difference between measurement and actual). We assume we include both here.

(4) Telescope pointing change & Build GMS LUT

- Key procedure:

  We repeat Step (3) at multiple zenith angles while M1CS is on. We build/update the GMS LUT for M2 and M3.

Table 2: Uncertainty after Step (3), Course alignment at Zenith

	Installation error	GMS error			Installation error
	M1 Segment	M2	M3	Instrument	Instrument
Rx	50 µrad	24 µrad	41 µrad	N/A	0.5 mrad$^+$
Ry	50 µrad	24 µrad	41 µrad	N/A	0.5 mrad$^+$
Rz	250 µrad	24 µrad	41 µrad	N/A	0 µrad
Tx	$160/\sqrt{2}$ µm	23 µm	23 µm	N/A	10 mm$^+$
Ty	$160/\sqrt{2}$ µm	23 µm	23 µm	N/A	10 mm$^+$
Tz	30 µm	23 µm	23 µm	N/A	10 mm

- Modeling assumption:

  A2 in Sec. 4.1 is assumed for the zenith angles. We assume that TCS has a perfect telescope pointing system and ignore any pointing errors associated with the telescope pointing to the sky angles.

(5) Telescope pointing change to ZA of 30 degree & star acquisition

- Key procedure

  While the M1CS is turned on, the TMT is pointed toward an acquisition star (a bright star) at the zenith angle of 30 degree. M2, M3 and APS are positioned according to the GMS LUT. A star is captured in the APS for the first time.

- Modeling assumption

  We assume the first star image is located within the APS image sensor capture range.

(6) APS measurement at the zenith angle of 30 degree

- Key procedure:

  At the zenith angle of 30 degree, APS measures, computes and applies the positions for the M1 segments PTT, WH commands, M2 PTT, and M3 TT. M1 WH commands are set once at the zenith angle of 30 degree, which are unchanged until next updates.

- Modeling assumptions :

  In addition to ***A3*** in Sec. 4.1, we list our additional assumptions regarding the APS measurement below. First, we assume the APS segment phasing algorithm meets its requirement of 6.8 nm by modeling 6.8 nm random segment piston as the phase algorithm error after ideal detection of segment piston. Second, The first 10 Singular Value Decomposition (SVD) modes are considered for control[15] with no knowledge error in Warping Harness Influence Functions (WHIFs). Third, we assume APS iterations are done twice. Fourth, when we capture Exit Pupil (ExP) position, we consider the "pupil position measurement uncertainty" of 1.5 mm over approximately 3 m ExP space. Lastly, when we capture star centroids at the image plane, we consider the "image position measurement uncertainty" of 0.05 arcsec On-Sky.

(7) Telescope pointing change & APS LUT

- Key procedure:

  We repeat Step (6) at multiple zenith angles while the M1CS is on. M1 segment out-of-plane DoF, PTT, are realigned, which provides new set points for the M1CS edge sensors. Based on these new set points, the M1CS fit formula is updated. The APS LUT is also updated for M2 and M3.

- Modeling assumption :

  A2 in Sec. 4.1 is assumed for the zenith angles. The APS literally has a LUT while the M1CS has a analytic formula to fit as a function of zenith angles instead of a LUT.

  While the telescope pointing changes, the M1CS is maintaining the segment out-of-plane motions and monitors the segment in-plane motions. Their set points (formula) are updated according to each zenith angle (and potentially temperature) measurement. The segment in-plane motions (translates and clocking) are perturbed due to thermal and gravitational error sources while ***A1*** is still true maintaining the out-of-plane motions.

  While the telescope pointing changes, the TCS (or M2CS/M3CSTBR) adjusts the 6 DoF M2 RB and M3 TT based on the GMS LUT first before the APS measurement.

(8) Finish alignment

- Key procedure:

  The alignment is finished. As a result, the APS LUT has WH actuator positions, M1 segment PTT, M2 PTT, M3 TT positions for the specified zenith angles as ***A2*** in Sec. 4.1. The M1CS finds set points (formula) for any arbitrary zenith angle.

(9) Instrument change

- Key procedure:
  M3 is repositioned to aim at a target instrument other than the APS.
- Modeling assumption :
  We only consider the Wide Field Optical Spectrometer (WFOS) in this study. No reliable gravity RB perturbation is available at this moment for other instrument. We assume that the WFOS has the same installation error as the APS (See Step(3)) with the same statistics but different realizations. We also assume the WFOS has the same gravity RB perturbation as the APS because there is no reliable study result available to us for the WFOS. The gravity motion of the WFOS is expected to be similar to that of the APS because they are located at the opposite sides of the TMT along the global y-axis.
  We consider several scenarios on how we position M2 and M3 when M3 is pointing to the WFOS as described later in Sec. 5.2, where the scenarios 3 (S3) is chosen as our baseline.

(10) OIWFS adjusts M2

- Key procedure:
  The OIWFS of the instrument measures and adjusts the M2 PTT during operations.
- Modeling assumption:
  See ***A5*** in Sec. 4.1.

5. RESULT

5.1 Baseline Scenario Results

Fig. 3 shows the resulting optical performance metrics for the baseline scenario at the APS location. The metrics include the rmsWFE after APS correction, the PSSN, the pupil shift, the star centroid , the plate scale distortion, and the plate scale distortion variation. Appendix A summarizes the definition of each metric.

We have built the four random realizations of TMTs. Then, we ran two different alignment processes for each TMT. The different colors in Fig. 3 are for four different TMT realizations. The different points are for two random alignment processes. The black curves in rmsWFE and PSSN plots are the average of those 8 different realizations.

According to the TMT Observatory Architecture Document (OAD),[10,16] the budgeted PSSN after the alignment is 0.85 at the zenith pointing angle of 30 degree. If we only consider the modeled terms listed in Table 1, the budgeted PSSN is 0.90327 at the zenith pointing angle of 30 degree, which is indicated as x in Fig. 3(b). We find the computed PSSN is better than this budgeted PSSN value. The black-dot curve in the PSSN plot is when ideal WFS is used rather than SH-WFS and with one of random realizations from the alignment study. By "ideal WFS", we mean we use the modeled OPD directly for sensing the wavefront shape. This method evaluates the theoretical limit of the wavefront control correction of the input error using the telescope control DoF. Note that the black-dot curve is worse than the alignment study result. The "ideal" phase-based wavefront sensor minimizes the rmsWFE as opposed to the SH-WFS method which minimizes the wavefront slope. It is interesting to note that although this phase-sensing method minimizes the wavefront error, the PSSN value is minimized using the slope-based approach, which is consistent to our previous study results.[15]

Note that M3 TT is adjusted at the considered zenith angles (***A2*** in Sec. 4.1) to minimize the ExP shift, the resulting pupil shifts are well centered to its controlled (or designed) position at the APS detector center. The pupil shift is dominated by the APS ExP measurement uncertainty of 1.5 mm over the around 3 m ExP space (Step 6 in Sec. 4) as shown in Fig. 3(c). The TMT Observatory Requirement Document (ORD)[17] requires the pupil shift is smaller than $\pm 0.3\,\%$ peak to valley of the pupil diameter. This requirement is indicated in Fig. 3(c). As shown in Fig. 3(c), the pupil shift meets the current requirement.

M3 TT compensates for the pupil position as shown in Fig. 3(c), but this results in star centroid error in the focal plane. For the different TMT realizations (different colors in Fig. 3(d)), the star centroids have an offset

dominated by the APS installation error and M2 GMS error. The gravity effect (elongation along x) is captured around 5 arcsec from 0 to 65 degree. This is mostly due to the instrument sliding along the gravitational axis as the gravity changes. The atmospheric TMT-noise is relatively small, which is indicated by separation of these dots in each realization (or same colored dots).

The star centroid is correlated to the plate scale distortion in Fig. 3(e). If the instrument and M2 are positioned closer to the optical axis (margenta and green dots), the plate scale distortion is relatively smaller than the others. Fig. 3(f) shows the plate scale distortion variation, which is residual after removing plate scale distortion offsets (See Appendix A). As shown in Fig. 3(f), the plate scale distortion variation meets the current requirement.

5.2 Various Scenario Results for WFOS

Fig. 4 shows the performance metrics after executing the alignment plan for the WFOS. Blue curves in rmsWFE and PSSN plots (Fig. 4(a) and (b) respectively) are same as the average cases in the APS baseline case in Fig. 3. For each random realization, we turn M3 to point to the WFOS. All results are based on four different TMT realizations and two different alignment realizations as in Fig. 3. (Total eight random realizations.)

We assume WFOS gravity-induced RB errors are same as APS as discussed in Step (9) in Sec. 4.2, which will be updated after we receive the instrument dependent perturbations. Note the magnitude of these errors is

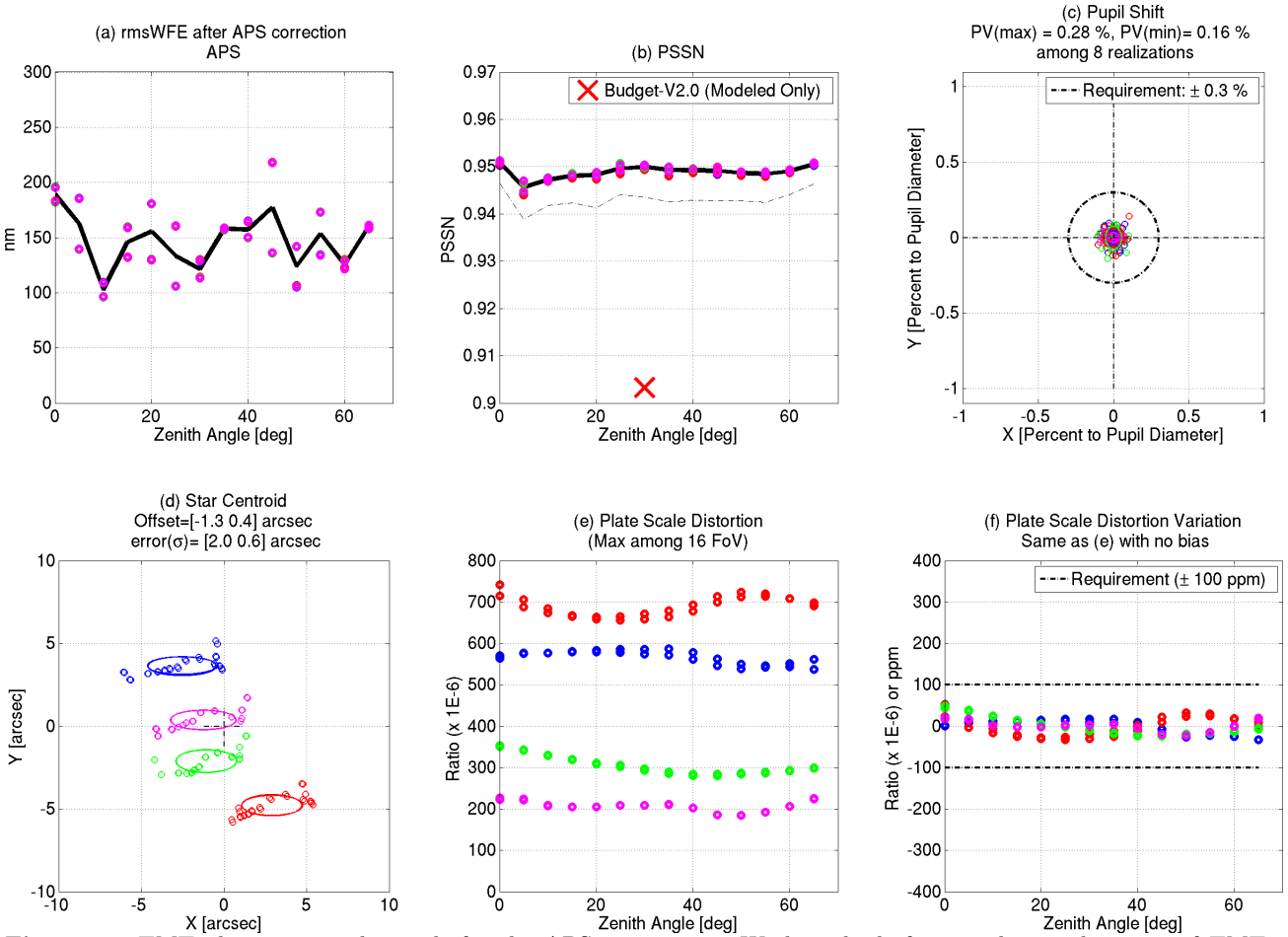

Figure 3: TMT alignment study result for the APS instrument: We have built four random realizations of TMTs. Then, we ran two different alignment processes for each TMT. The different colors are for four different TMT realizations. The different points are for two random alignment processes and 14 zenith angles considered. The black curves in rmsWFE and PSSN plots are average of those 8 different realizations.

not dominant. It is comparable to the M3 GMS error, affecting the pupil position error, the pointing error and the distortion error, but not affecting the rmsWFE and the PSSN. Same statisics but different realizations of installation errors are considered for the WFOS and the APS as discussed in Step (9) in Sec. 4.2.

After switching to WFOS from the APS instrument by repointing M3, we study following different scenarios in positioning M2 and M3.

(S1) **Scenario 1: APS LUT for M2, APS LUT for M3**:

In this scenario, we position M2 6 DoF from the GMS LUT followed by the APS LUT as it would be for the APS. In terms of M3 TT, there are three LUTs. They are *M3/GMS@WFOS LUT*, *M3/GMS@APS LUT*, and *M3/APS LUT*.

The *M3/GMS@WFOS LUT* and *M3/GMS@APS LUT* are the GMS measurement of M3 at the WFOS and the APS locations respectively. The *M3/APS LUT* is the APS measured position of the M3 TT and captures the delta motion of M3 TT from *M3/GMS@APS* to optimize the pupil position at the APS location.

In this scenario, when switching to WFOS from APS, we first use *M3/GMS@WFOS* for M3 and apply *M3/APS LUT* to align M3 TT. When applying *M3/APS LUT* at WFOS, we consider the geometric difference of the instrument location (WFOS and APS are located at the exactly opposite side) on the telescope.

This scenario would be best if there is no instrument-dependent error or no random errors between the APS and the WFOS since we are utilizing the APS measurement directly.

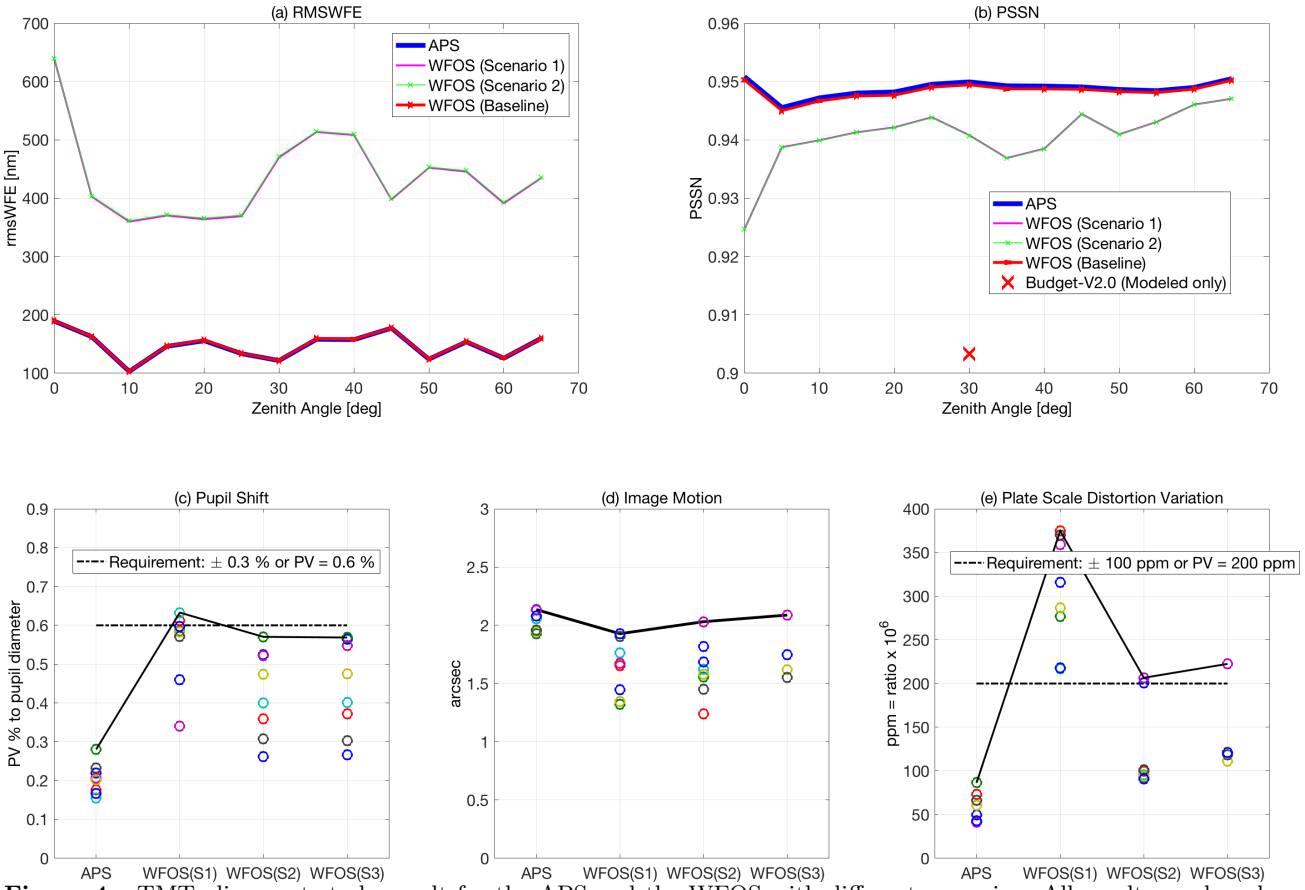

Figure 4: TMT alignment study result for the APS and the WFOS with different scenarios. All results are based on four different TMT realizations and two different alignment realizations as in Fig. 3. (Total eight random realizations.)

(S2) **Scenario 2: APS LUT for M2, GMS LUT for M3**:

The scenario 2 is same as (S1) except we use *M3/GMS@WFOS* for M3 TT but do not apply *M3/APS LUT* to align M3 TT. This scenario 2 is not relying on the APS measurement for M3, but still does for M2.

(S3) **Scenario 3: OIWFS for M2, GMS LUT for M3**:

The scenario 3 is same as (S2) except we use the OIWFS for M2 at WFOS. This scenario 3 is not relying on any of the APS measurements for M2 and M3.

Note that the source of the GMS measurement errors, instrument installation errors, and APS measurement errors are random. The gravity-induced instrument RB errors are the only deterministic error source. If the random errors are dominant over the deterministic errors, (S3) and (S2) would be better choices over (S1). As shown in Fig. 4, (S3) is best and becomes our baseline for the WFOS instrument.

Fig. 4(a) and (b) show that the rmsWFE and the PSSN in (S1) and (S2) are worse than those of APS and (S3). The dominant reason is because of the instrument installation error discussed in Table 1, which introduces dominant defocus in (S1) and (S2). Once the OIWFS is used at the WFOS, M2 PTT is adjusted to compensate this instrument installation error and the gravity-induced RB errors, resulting the residual rmsWFEs and PSSNs are similar between APS and WFS (S3). Therefore, an OIWFS is needed for the WFOS (or each instrument). Without it, a PSSN loss of 0.01 is expected. Note that we assume an OIWFS is located On-Axis as discussed in ***A2*** in Sec. 4.1 thus, we do not capture the potential off-axis effect of OIWFS location. In future work, we will repeat this study with an OIWFS positioned Off-Axis.

The difference between APS and WFOS (S3) is mostly due to the M3 figuring error. When the APS minimizes the ExP WFE, M1 segments PTT and WH actuators are optimized at the APS location, where the WFE includes the spatially random M3 figuring error. If we turn M3 away from the APS, M1 segments correction on the M3 figuring error becomes wrong making the WFE worse. If M3 figuring error is white spatial noise and the spatial control bandwidth is high enough, the rmsWFE and the PSSN degradation would be factor of $\sqrt{2}$ and 2 of the M3 figuring error, respectively. Since CBE of the M3 figuring error is approximately 0.999, the PSSN difference is smaller than 2×10^{-3}. Note that the PSSN of the WFOS is expected to be worst in terms of M3 figuring error correction among all instruments since it is located furthest from APS. On the other hand, spatially symmetric errors are reasonably well corrected in the WFOS such as the M3 passive support error.

The pupil shift at the APS is affected by several error sources. Eq. (1) symbolically represents the pupil position error at the APS.

$$\text{APS pupil shift} = M3/GMS@APS + APS/GE - (M3/GMS@APS + APS/GE) + [N_m] \tag{1}$$

, where "M3/GMS@APS" represents M3 GMS measurement error at the APS, "APS GE" represents the APS gravity-dependent RB error, "(M3/GMS@APS + APS GE)" represents the pupil position correction by the APS moving M3 TT, and N_m is the pupil correction sensing and control error. "[ ]" indicates the dominant error. Note that the pupil error is dominated by N_m at the APS.

Likewise, we can formulate the pupil errors for S1, S2, and S3 for the WFOS as Eq. (2).

$$\begin{cases} \text{WFOS pupil shift (S1)} & = [M3/GMS@WFOS] + WFOS/GE - ([M3/GMS@APS] + APS/GE) + N_m \\ \text{WFOS pupil shift (S2)} & = [M3/GMS@WFOS] + WFOS/GE \\ \text{WFOS pupil shift (S3)} & \approx \text{(S2)} \end{cases} \tag{2}$$

In (S1), $M3/GMS@WFOS$ and $WFOS/GE$ are applied instead of $@APS$. Since we employ the same APS LUT for this scenario, "(M3/GMS@APS + APS GE)" is still used like the APS case. It is our assumption that WFOS and APS have the same gravity-dependent RB error, that is $WFOS/GE = APS/GE$. Then, we find that difference between M3 RB GMS measurement between WFOS and APS is the dominant source for (S1), that is $M3/GMS@WFOS - M3/GMS@APS$. Because we assume the GMS measurement error is independent

between the two instruments, the subtraction in $M3/GMS@WFOS - M3/GMS@APS$ is statistically making the pupil shift worse.

In (S2), $M3/GMS@WFOS$ and $WFOS/GE$ are still the same as (S1). We simply remove the correction done by the APS LUT. We find that the M3 GMS measurement error, $M3/GMS$, is larger than the gravity-induced RB errors for APS and WFOS. Therefore, the M3 GMS errors is the dominant source for (S2), that is $M3/GMS@WFOS$. (S3) is almost same as (S2) because M2 PTT position adjustment done in (S3) is not very sensitive to the the pupil position change.

As a summary, the dominant error source of the pupil shift in the baseline WFOS scenario (S3) is the M3 GMS measurement error. This implies that the benefit from using the APS LUT at WFOS to compensate the deterministic error (gravity-induced instrument) is small compared to the random GMS errors.

The maximum peak-to-valley pupil shift among 8 realizations is very close to its requirement as shown in Fig. 4(c), implying the requirement is very tight. We also find the plate scale distortion variation is close to its rquirement as shown in Fig. 4(e).

6. CONCLUSION AND FUTURE WORK

Alignment modeling performed in this paper has been directed towards understanding the telescope alignment while taking into account initial telescope deformations, gravity deformation and initial installation tolerances. As a result, we find the image quality metric, PSSN, meets current requirements after alignment at both APS and WFOS locations. We also report other metrics such as the pupil shift, the plate scale distortion and the image motion.

The study also considers three different alignment strategies using combinations of GMS LUT, APS LUT and OIWFS feedback. Based on the computed metrics, we propose a baseline alignment strategy for instruments other than APS; M3 position is determined by the GMS and M2 position is determined by OIWFS feedback. The PSSN at the WFOS instrument is improved by 0.01 if an OIWFS is used. The pupil shift meets its requirement of $\pm$ 3 %[17] but with very tight margin if M3 position is determined by the GMS measurement for the WFOS. In order to gain some margin for the pupil shift, the GMS accuracy on M3 needs to be improved or the WFOS (or eahc instrument) needs to have a method to sense the pupil location to adjust M3 TT.

As the initial and installation errors are static and the zenith angle dependent defections are repeatable, the results are affected only by the APS and the OIWFS measurement uncertainty, GMS measurement uncertainty, accuracy of LUTs to fit to zenith angle dependent errors and the assumed alignment strategy. It is our plan to update the current results as our knowledge become more mature to support the TMT system engineering group. We conclude our report by listing our near-term future tasks. First, we will consider additional errors including non-repeatability (hysteresis) of actuators, manufacturing tolerances of the telescope structure causing zenith angle dependent effects, gravity and tolerance effects within subsystems, and temperature dependent effects. Second, we will expand our scope of performance evaluation by exploring more instruments and off axis FoV performance.

APPENDIX A. DEFINITION OF METRICS

We define the metrics used in the paper below.

- **Normalized Point Source Sensitivity (PSSN)**:
  PSSN is the seeing limited optical performance metric for TMT. We have studied the effects of the PSSN metric in detail in [18, 19]. PSSN is the (inverse) Signal-to-Noise Ratio (SNR) normalized to that of the perfect telescope looking through the same atmosphere. PSSN essentially quantifies the science loss for seeing limited instruments in terms of required increase in integration time. According to TMT OAD, PSSN is required to be 0.85 and better. This translates to 17.6% longer integration time relative to a perfect system. (The integration time scales by 1/PSSN.) to reach the same SNR. For this study, 500 nm is used for the baseline wavelength, 200 mm is used for the atmospheric Fried-Parameter r_o when TMT is pointing to zenith.i.e., r_o is adjusted due to telescope pointing zenith angle.

- **Pupil position**:
  The nominal ExP is placed at the "Pupil Plane", which is just behind M2 if we ignore the folding at M3. We use our ray-tracing tool, Modeling and Analysis for Controlled Optical Systems (MACOS),[20] to compute the ExP with and without any perturbation. "Pupil position" is computed as the delta of the two positions and represented in x,y,z in the pupil plane local coordinate system.
- **Pupil position offset**:
  The pupil position depends on the zenith angle if TMT is perturbed. "Pupil position offset" is computed as the mean of the pupil position for zenith angles between 5 and 65 degree.
- **Pupil shift**:
  "Pupil shift" is computed as the residual of the pupil position after removing the pupil position offset. The TMT ORD[17] requires the pupil shift is smaller than $\pm 0.3\,\%$ peak to valley of the pupil diameter.
- **Star Centroid**:
  "Star centroid" is the centroid of a bundle of rays at the focal plane on a given Sky FoV. We use MACOS to compute the On-Axis star centroid with and without any perturbation. "star centroid" is computed as the delta of two positions and represented as x,y in focal plane local coordinate system. See our assumption, ***A6*** in Sec. 4.1, in terms of the telescope pointing model.
- **Star Centroid fit**:
  The star centroid depends on the zenith angle if TMT is perturbed. "Star Centroid fit" is the 3rd order polynomial fit as a function of zenith angle for the On-Axis star centroids considering the zenith angle between 5 and 65 degree.
- **Star Centroid error**:
  "Star centroid error" is computed as star centroid residual after star centroid fit is removed from the star centroid.
- **Image motion**:
  "Image motion" is computed as the standard deviation of the On-Axis star centroid error in radial direction for zenith angle between 5 and 65 degree.
- **Plate scale distortion**:
  We first define the 17 FoV positions on the sky as described in Fig. 5. We use MACOS to compute the star centroids for those 17 FoV with and without any perturbation. Note that On-Axis perturbation is the same as the star centroid. Next, we remove the On-Axis x and y offset (or On-Axis star centroid) commonly for all FoV. Then, we take the ratio of the delta centroid spot to the nominal field offset at each FoV. "Plate scale distortion" is defined as the maximum of the ratio among those 16 FoV except the On-Axis position.
- **Plate scale distortion variation**:
  "Plate scale distortion variation" is defined as the residual of the plate scale distortion after removing the plate scale distortion offset, which is the mean of the plate scale distortion for the zenith angles between 5 and 65 degree. The TMT ORD[17] requires the "plat scale uniformity" to be smaller than 0.06 arcsec, which is defined as any change of the plate scale over any length of time at any field point. The 0.06 acrsec corresponds 100 ppm change at the edge of the FoV. We interpret this requirement as an upper bound for the plate scale distortion variation.

ACKNOWLEDGMENTS

The research was carried out in part at the Jet Propulsion Laboratory, California Institute of Technology, under a contract with the National Aeronautics and Space Administration. The authors gratefully acknowledges the support of the TMT collaborating institutions. They are the California Institute of Technology, the University of California, the National Astronomical Observatory of Japan, the National Astronomical Observatories of China and their consortium partners, the Department of Science and Technology of India and their supported institutes, and the National Research Council of Canada. This work was supported as well by the Gordon and Betty Moore Foundation, the Canada Foundation for Innovation, the Ontario Ministry of Research and Innovation, the Natural Sciences and Engineering Research Council of Canada, the British Columbia Knowledge Development Fund, the Association of Canadian Universities for Research in Astronomy (ACURA), the Association of Universities for Research in Astronomy (AURA), the U.S. National Science Foundation, the National Institutes of Natural Sciences of Japan, and the Department of Atomic Energy of India.

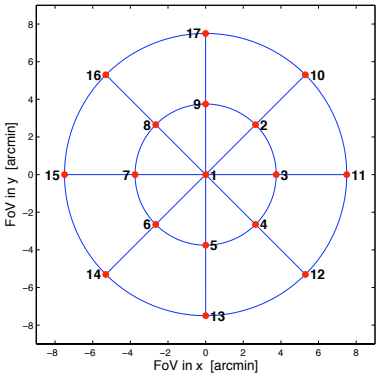

ID	x-FoV [arcmin]	y-FoV [arcmin]	ID	x-FoV [arcmin]	y-FoV [arcmin]
01	0.0000	0.0000			
02	2.6517	2.6517	10	5.3033	5.3033
03	3.7500	0.0000	11	7.5000	0.0000
04	2.6517	-2.6517	12	5.3033	-5.3033
05	0.0000	-3.7500	13	0.0000	-7.5000
06	-2.6517	-2.6517	14	-5.3033	-5.3033
07	-3.7500	-0.0000	15	-7.5000	-0.0000
08	-2.6517	2.6517	16	-5.3033	5.3033
09	-0.0000	3.7500	17	-0.0000	7.5000

Figure 5: 17 FoV positions for plate scale distortion evaluation. Unvignetted telescope FoV (15 arcmin).

REFERENCES

1. C. Nissly, B. Seo, M. Troy, G. Angeli, J. Angione, I. Crossfield, B. Ellerbroek, L. Gilles, N. Sigrist, and L. Wang, "High-resolution optical modeling of the Thirty Meter Telescope for systematic performance trades," *Proc. SPIE*, vol. 7017, p. 70170U, June 2008.
2. C. Nissly, B.-J. Seo, M. Troy, G. Angeli, M. Cho, B. Ellerborek, P. Piatrou, L. C. R. Jr., C. Shelton, and L. Wang, "High fidelity optical modeling for TMT," *Proc. SPIE*, vol. 7017, p. 10, Aug 2011.
3. C. Nissly, B.-J. Seo, M. Troy, G. Chanan, S. Roberts, and J. Rogers, "Wavefront sensing and control performance modeling of the thirty meter telescope for systematic trade analyse," *Proc. SPIE*, vol. 9150, Aug 2014.
4. C. Nissly, B.-J. Seo, and M. Troy, " JPL Optical Modeling Error Manual (V2.4) ," *TMT Project Communication*, vol. TMT.SEN.TEC.13.003.DRF05, 5 2018.
5. "Estimate of GMS Accuracy," *TMT Project Communication*, vol. TTMT.SEN.TEC.16.012.DRF01, Feb. 2016.
6. G. Chanan, M. Troy, and I. Crossfield, "Predicted measurement accuracy of the TMT Alignment and Phasing System," *TMT Project Communication*, vol. TMT.CTR.PRE.07.007.REL01, Feb 2007.
7. M. Troy, G. Chanan, S. Michaels, F. Dekens, R. Heins, S. Herzig, R. Karban, C. Nissly, J. Roberts, M. Rud, and B.-J. Seo, "The alignment and phasing system for the thirty meter telescope: risk mitigation and status update," *Proc. SPIE*, vol. 99066A, July 2016.
8. D. G. MacMynowski, P. Thompson, J. C. Shelton, L. C. Roberts, M. M. Colavita, and M. J. Sirota, "Control system modeling for the Thirty Meter Telescope primary mirror," *Proc. SPIE*, vol. Integrated Modeling of Complex Optomechanical Systems Symposium, Aug 2011.
9. C. Shelton and L. C. Roberts, "How to calibrate edge sensors on segmented mirror telescopes," *Proc. SPIE*, vol. Ground-based and Airborne Telescopes IV, September 2012.
10. S. Roberts and J. Rogers, "Image Quality Error Budget R20," *TMT Project Communication*, vol. TMT.SEN.DRD.07.026.REL20, Jan 2016.
11. G. Chanan, "Design of the Keck Observatory alignment camera," *Proc. SPIE*, vol. 1036, p. 59, 1988.
12. TMT, "TMT Coordinate Systems and Transfroms," *TMT Project Communication*, vol. TMT.SEN.TEC.07.031.DRF03.
13. E. Williams, "SSA System Level Calculations," *TMT Project Communication*, vol. TMT.OPT.TEC.08.054.REL03, May 2015.
14. "ICD-STR-NFIRAOS," *TMT Project Communication*, vol. TMT.AOS.ICD.07.004.CCR13, June 2015.
15. B. Seo, C. Nissly, G. Angeli, D. MacMynowski, N. Sigrist, M. Troy, and E. Williams, "Investigation of primary mirror segment's residual errors for the Thirty Meter Telescope," *Proc. SPIE*, vol. 7427, Aug. 2009.
16. TMT, "TMT Observatory Architecture Document," *TMT Project Communication*, 12 2013.
17. TMT, "TMT Observatory Requirement Document," *TMT Project Communication*, 5 2017.

18. B.-J. Seo, C. Nissly, G. Angeli, B. Ellerbroek, J. Nelson, N. Sigrist, and M. Troy, "Analysis of Normalized Point Source Sensitivity as Performance Metric for Large Telescopes," *Applied Optics*, vol. 48, pp. 5997–6007, 2009.
19. B. Seo, C. Nissly, M. Troy, and G. Angeli, "Normalized point source sensitivity for off-axis optical performance evaluation of the Thirty Meter Telescope," *Proc. SPIE*, vol. 7738-16, June 2010.
20. D. Redding *et al.*, "MACOS manual (Modeling and Analysis for Controlled Optical Systems)," *NASA JPL D-9816, internal document*, vol. 5, 1999.